Estuarine, Coastal and Shelf Science 161 (2015) 11–24

Contents lists available at ScienceDirect

Estuarine, Coastal and Shelf Science

journal homepage: www.elsevier.com/locate/ecss

Field and laboratory observations of bed stress and associated nutrient release in a tidal estuary

Meagan E. Wengrove [a, *], Diane L. Foster [b], Linda H. Kalnejais [c], Vincent Percuoco [c], Thomas C. Lippmann [d]

[a] Department of Civil and Environmental Engineering, University of New Hampshire, Durham, NH, United States
[b] Department of Mechanical Engineering, University of New Hampshire, Durham, NH, United States
[c] Department of Earth Sciences and Institute for the Study of Earth, Oceans, and Space, University of New Hampshire, Durham, NH, United States
[d] Department of Earth Sciences and Center for Coastal & Ocean Mapping, University of New Hampshire, Durham, NH, United States

ARTICLE INFO

Article history:
Received 12 April 2014
Accepted 15 April 2015
Available online 29 April 2015

Keywords:
sediment resuspension
sediment erosion
sediment nutrient release
excess shear stress
estuarine geochemistry
benthic-pelagic coupling

ABSTRACT

Nutrient release driven by sediment resuspension in a shallow coastal estuarine system is examined with field observations of bed stress and bed elevation, coupled with laboratory erosion experiments on sediment cores. Two field experiments were conducted over near-cohesive muddy-sand sediments in the Great Bay Estuary, New Hampshire. In the first deployment, boundary layer development during typical summer tidal forcing was observed, while the second deployment occurred under enhanced wind forcing of Tropical Storm Irene. *In situ* bed stress and erosion depths were estimated with a profiling acoustic Doppler velocimeter. Sediment cores were subjected to EROMES erosion chamber experiments to determine erosion depth and nutrient release as a function of applied shear stress. Results show erosion depths are consistent with *in situ* observations over shear stresses ranging from 0.10 N m^{-2} (incipient motion) to 0.35 N m^{-2} (resuspension events). Erosion chamber experiments showed that ammonium release (up to 2 mmol m^{-2}) increased with bed stress in both spring and summer. However, phosphate release was more variable, with no phosphate release during resuspension in spring and a variable phosphate flux (ranging −0.5–2 mmol m^{-2}) in summer. Increased hydrodynamic forcing during a storm event in the summer generated shear stresses (up to 0.58 N m^{-2}) during flood tides that exceeded the threshold for sediment motion, and resulted in erosion of the seabed. EROMES results predict there was concomitant release of nutrients into the water column from the muddy sediments of the Bay, and the release of dissolved inorganic nitrogen and phosphate was up to 10% and 65%, respectively, of the summer monthly riverine input of these nutrients. Results indicate qualitatively that in shallow, tidally dominated estuaries, fine-grained sediment beds may be a source of nutrients that are particularly important during storms that enhance near bed shear stresses.

1. Introduction

Excess nutrients in coastal waters can significantly impact the water quality and aquatic ecosystems by increasing primary productivity, and altering community structure (Cloern, 2001). Consequently, there is continued worldwide interest to mitigate these effects by reducing the input of nutrients to coastal waters (Boesch, 2002). In estuaries with large nutrient loads from rivers and/or high suspended sediment concentrations, the lateral advection component is generally assumed to be the dominant source of nutrient concentrations (Jay et al., 1997). However, in regions where there are fine grained sediments and intermittently large flows, the vertical flux of nutrients into and out of the sediment beds can significantly affect the nutrient budget (Jay et al., 1997; Kornman and de Deckere, 1998; Lorke et al., 2003). Organic matter that accumulates in fine-grained sediments can be remineralized, producing nutrients that can be returned to the water column (Giblin et al., 1997). In Chesapeake Bay, Maryland (Boynton and Kemp, 1985), and Mobile Bay, Alabama (Cowan et al., 1996), release from sediments has been estimated to supply over 25% of the dissolved nutrients for phytoplankton growth, and in Galveston

* Corresponding author. Current address: Department of Ocean Engineering, University of New Hampshire, 24 Colovos Road, Durham, NH, United States.
E-mail addresses: meagan.wengrove@gmail.com, med36@wildcats.unh.edu (M.E. Wengrove).

http://dx.doi.org/10.1016/j.ecss.2015.04.005
0272-7714/

Bay, Texas (Warnken et al., 2000) sediments were found to be the dominant source of nutrients to the Bay.

Despite sediments being a potentially large repository of nutrients, their influence upon the nutrient budget in coastal waters is often poorly quantified (Couceiro et al., 2013). The release of nutrients from sediments to the water column depends not only on sediment geochemistry, but also on local hydrodynamics (Lorke et al., 2003). Sediment geochemistry determines the reactions that produce nutrients from remineralization, as well as the reactions that remove nutrients, such as denitrification or phosphate mineral precipitation. Hydrodynamic stresses applied to the bed affect the suspension of sediments and rate of exchange of solutes across the sediment–water interface, which in turn influences the sediment geochemistry by controlling the supply of key reactants, and the release of dissolved products. At the bed interface, exchange can occur as a result of vertical diffusion as well as resuspension of sediment and accompanying pore water (Jorgensen and Revsbech, 1985; Hondzo, 1998). The rate of exchange or vertical flux is determined by the boundary layer dynamics, sediment erosion threshold, and the chemistry of the overlying water (Boudreau and Jorgensen, 2001; Lorke et al., 2003; Sanford and Maa 2001; Couceiro et al., 2013).

Most previous research efforts have quantified release of nutrients under quiescent conditions. Calculation of the vertical flux from porewater profiles often assumes molecular diffusion is the dominant mixing mechanism. Direct flux measurement techniques such as benthic chambers (Warnken et al., 2000; Berelson et al., 2003) and core incubations (Fulweiler et al., 2010; Tucker et al., 2014) provide valuable measurements of nutrient flux but generally isolate the overlying fluid, thereby altering the boundary layer dynamics. Chambers and incubations typically use a single stirring speed to circulate the overlying fluid, providing flux observations for a single flow condition that is usually selected to ensure no sediment is resuspended. Interpretation of these results is therefore limited due to highly dynamic and variable flow conditions present in coastal waters. When the flow field exceeds the threshold for rough turbulent flow, the diffusion due to turbulence significantly exceeds viscous contributions and the diffusive flux can be increased by more than an order of magnitude (Hondzo, 1998; Lorke et al., 2003; Wengrove and Foster, 2014). Moreover, nutrient exchange across the sediment–water interface may be further enhanced when the shear stress exceeds the erosion threshold and sediment is mobilized into the water column (Tengberg et al., 2003; Kalnejais et al., 2010; Kleeburg and Herzog, 2014). Nutrient release during resuspension can be due to entrainment of sediment and porewaters into the water column and also due to reactions of freshly suspended particles (Kalnejais et al., 2010; Couceiro et al., 2013).

Owing to challenges involved in making measurements of nutrient release under strong flow conditions, erosion devices designed to simulate sediment resuspension have been simultaneously used to investigate nutrient release (Sloth et al., 1996; Tengberg et al., 2003; Almroth et al., 2009; Kalnejais et al., 2010; Couceiro et al., 2013; Kleeburg and Herzog, 2014). These devices impose a known shear stress at the sediment–water interface, and sampling of the overlying fluid allows for evaluation of both erosion and local chemical transformations associated with a range of shear stresses. In situ determination of sediment erodibility prevents sediment disturbance associated with coring, and there are a number of *in situ* erosion devices (e.g. Amos et al., 1992; Widdows et al., 2007; Thompson et al., 2011, 2013). However, *in situ* determinations of nutrient release in the marine environment are limited (Tengberg et al., 2003; Almroth et al., 2009) and typically have been restricted to a single level of resuspension. Erosion chamber experiments performed in the laboratory on freshly collected cores (Koschinsky et al., 2001; Kalnejais et al., 2010; Couceiro et al., 2013) have provided information on nutrient release across a wider range of shear stresses. With climate change predicted to increase the number of extreme events in many regions the use of erosion devices to determine erosion response and associated chemical release is becoming increasingly important (Statham, 2012). Unfortunately, interpretation of erosion chamber results are hampered by poor comparisons between devices (Tolhurst et al., 2000b; Widdows et al., 2007) and lack of direct comparison between erosion chamber results and field observations (Andersen et al., 2007). Robust validation of the chambers requires high resolution observations of the velocity field, as a proxy for *in situ* shear stress, in the lowest few centimeters of the water column, with concomitant observation of sediment erosion.

In this work, field observations of near bottom fluid velocities and seabed elevation changes are used to assess the accuracy of the erosion threshold and depth determined by an EROMES erosion chamber. The field observations are coupled with erosion chamber measurements of nutrient release from muddy sites within the Great Bay estuary, New Hampshire, USA to provide information on nutrient mixing across the sediment–water interface in a shallow, temperate estuary. Field observations were obtained under typical non-storm (low winds) conditions where there was no evidence of sediment resuspension, and during a storm (high winds) when there was a fully rough turbulent boundary layer and active resuspension. The objectives of this paper are to 1) observe the fine-scale velocity structure near the seabed and concurrent bed elevation changes in estuarine field experiments, 2) verify theoretical critical shear stress values for sediment mobilization, 3) verify the accuracy of the EROMES erosion chamber and 4) relate the field-estimated shear stresses to nutrient release through coupled laboratory erosion chamber experiments. This study provides a significant step towards the validation of the erosion characteristics simulated by an erosion chamber with in-situ measured erosion rates and estimated shear stress. Additionally, the pairing of *in situ* hydrodynamic and erosion observations during a moderate storm and estimates of the magnitude of benthic nutrient release at increasing erosion thresholds show that resuspension events may be important terms in the nutrient budget of shallow estuarine systems.

2. Materials and methods

2.1. Field site

Field observations were obtained in the Great Bay Estuary (Fig. 1), a shallow well-mixed estuary with a (generally) sub-critical flow regime (Swift and Brown, 1983; Bilgili et al., 2005). Bottom sediment type is roughly correlated to water depths with grain sizes ranging from fine grained cohesive muds to coarse grained sands (Fig. 2). Spatial variability of sediment type is evaluated with both a depth model and with historic grab samples. In the first method, surficial mud fraction is estimated with a logarithmic model based on water depth and calibrated with observed sediment size fractions in the Little Bay portion of the Great Bay (Fig. 2b). The model has a correlation of 0.67, accounting for 44% of the variance (Lippmann, 2013). In the second method, historical sediment data (Poppe et al., 2003) is qualitatively discretized into regions of similar sediment type within the Bay (Fig. 2c). Sediment type is classified into four categories based on sediment size: mud, muddy-sand, sandy-mud, and sand following Shepard (1954) in Table 1.

The Great Bay is showing several symptoms of eutrophication, including substantial loss of eelgrass beds and macroalgae growth (Short and Wyllie-Echeverria, 1996; PREP, 2013), and there is

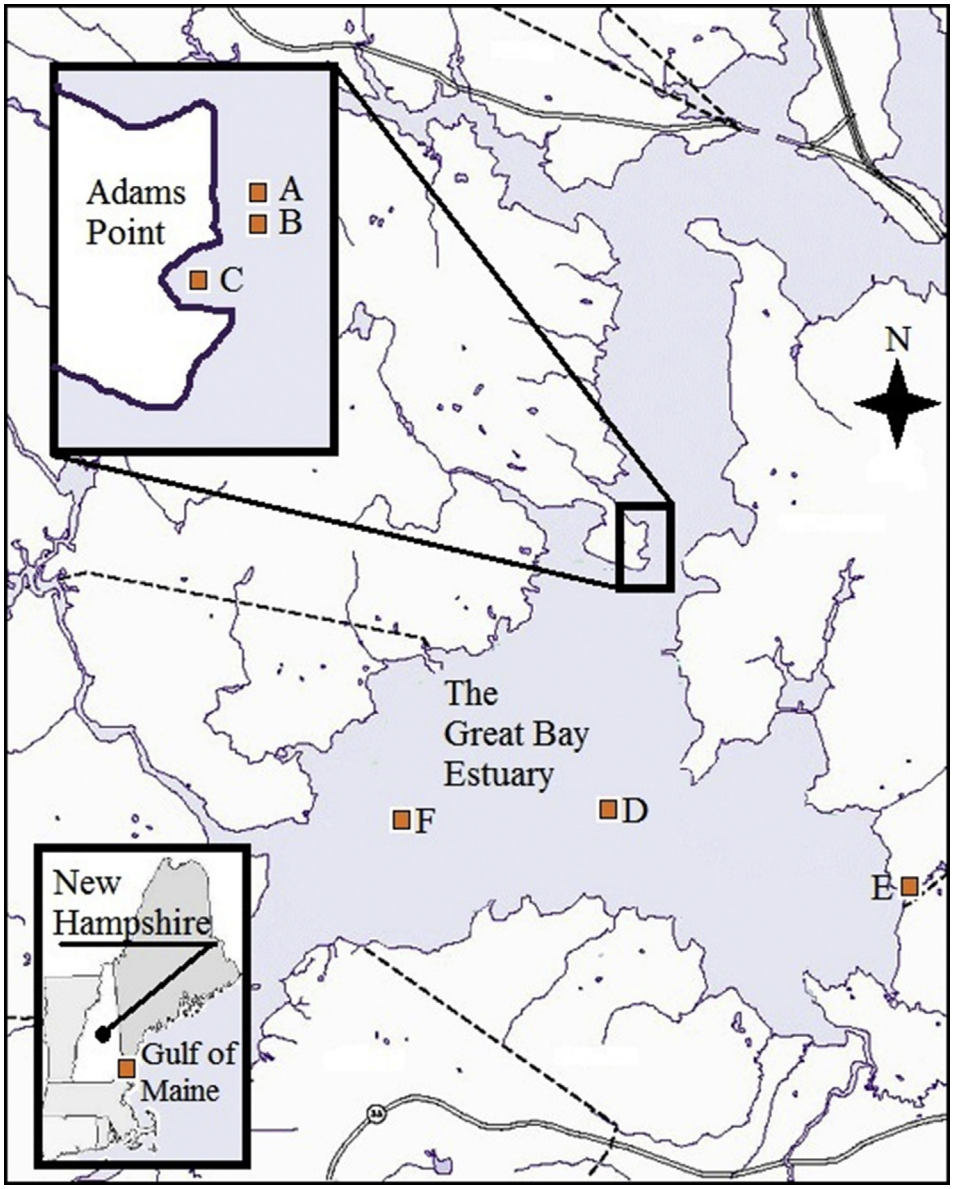

Fig. 1. Map of the Great Bay Estuary with instrument and sampling locations indicated. (A) The hydrodynamic field sampling array location (Latitude: 43.093° N, Longitude: 70.865° W) and the Tropical Storm Irene sediment core collection site (cores Irene1 and Irene2). This the sampling array was located within a long straight channel leading from the Little Bay to the Great Bay at Adams Point. Flow during the flooding tides is South at the sampling location. (B) Salinity sampling site during Tropical Storm Irene. (C) JEL sampling site for erosion chamber and geochemistry cores for June and August. (D) Location of the Great Bay Buoy, deployed during the spring to early fall months, used for local wind data during both the non-storm and storm deployments. (E) Location of the Great Bay Environmental Monitoring Network used for historical local wind data. (F) SQM geochemistry sampling site.

considerable interest in resolving the nutrient cycling within the Bay. An active monitoring program obtains measurements of nutrient concentrations in the major tributaries and within the Bay (PREP, 2013). Concentrations are generally attributed to local land use practices and wastewater treatment plant release through its tributaries and there is no consideration of the nutrients stored in or released from the sediments in the nutrient budget of the bay.

The *in situ* observations were obtained from a site located near the University of New Hampshire Jackson Estuarine Laboratory at Adams Point (Fig. 1). The semi-diurnal tide at the field site ranges 2–4 m over spring-neap cycles, and during typical conditions the dominant hydrodynamic contribution to the Bay is from tidal flows (Bilgili et al., 2005). *In situ* hydrodynamic observations were obtained at a mean water depth of 2 m. Wind speed during the sampling periods was measured from the Great Bay buoy 2.5 km away from the sampling location (Fig. 1) (CICEET, 2011). Historical 15 min interval averaged wind speeds from 2007 to 2011 were obtained from a meteorological station maintained by the Great Bay Environmental Monitoring Network in Greenland, New Hampshire, approximately 4.8 km from the field site (CICEET, 2011).

The median grain size diameter, d_{50}, at the hydrodynamic sampling location (Adams Point) is 113 μm, and at the sediment nutrient release sampling location (JEL) is 47 μm, thus the sediment was classified as a muddy-sand and a sandy-mud, respectively, based on the Shepard classification (Shepard, 1954) determined by the distribution of sediment grain size and the USGS Grain Size Chart (USGS, 2005). The breakdown of sediment composition and corresponding classification at the sampling locations are shown in Table 1. Although the sediment distribution at Adams Point technically puts the site in a non-cohesive sediment category, the

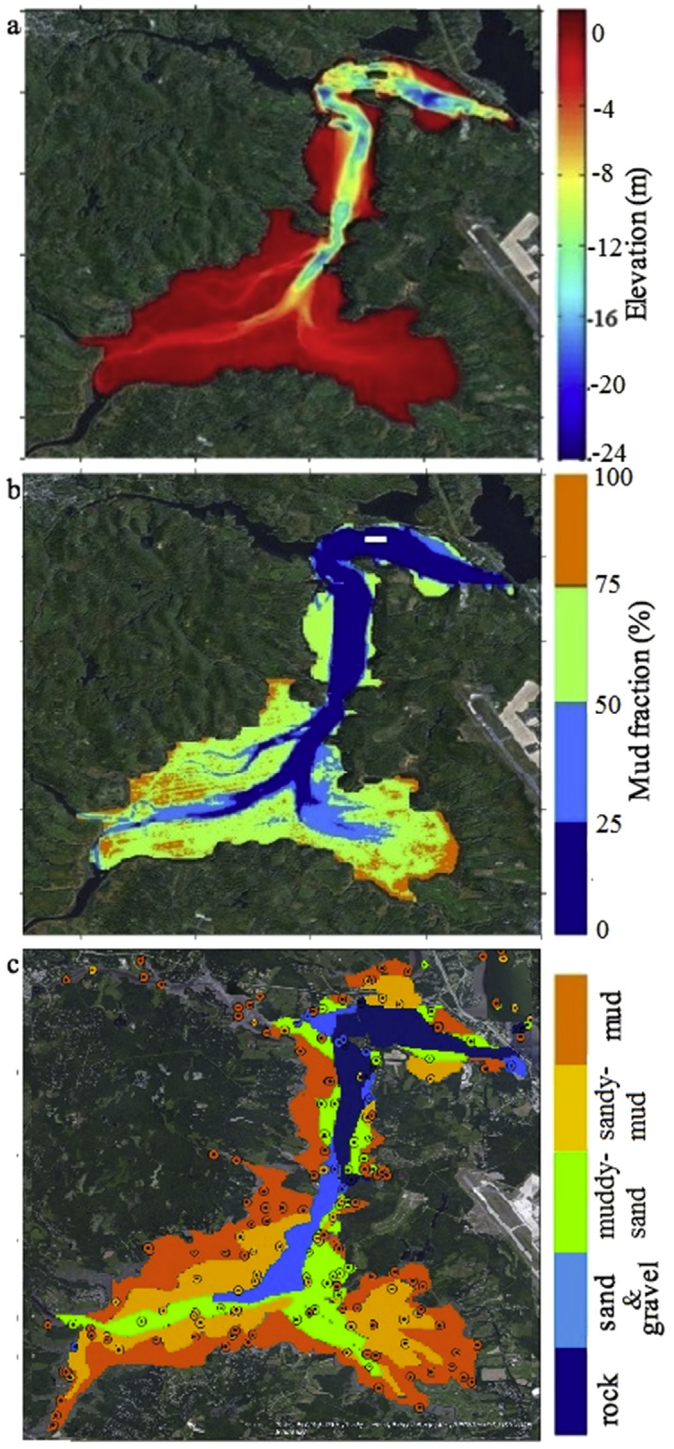

Fig. 2. (a) Water depth map of the Great Bay system. (b) Sediment distribution map of the Great Bay system based on a mud fraction model developed in the Little Bay using measurements of water depth related to sampled sediment mud fraction (Lippmann, 2013). Method indicates that 58% of Bay sediment has 50% mud or more. (c) Sediment distribution map of the Great Bay system as determined by qualitative interpolation (filled blocks) from existing historical sediment data (filled points) (Poppe et al., 2003). Method indicates that 55% of Bay sediment has 50% mud or more.

fraction of mud (25%) and very fine sand within the sediments results in a bed that exhibits cohesive tendencies (Mitchener et al., 1996). Incipient motion of sediment is generally assumed to occur when the shear stress, τ, exceeds its critical limit, τc (=0.1 for the Adams Point site; Shields, 1936). During non-storm conditions, the Shields parameter ($\tau < 0.09$) approached but did not exceed the critical threshold (Fig. 4d); however, during storm conditions, estimates of τ ranged between 0.2 and 0.6 and exceeded τc (Fig. 5d).

2.2. Instrumentation

The sampling array (Fig. 3a) for the hydrodynamic observations consisted of a single point acoustic Doppler velocimeter (Nortek Vector ADV) that sampled three components of velocity at 64 Hz, 80 cm above the boundary. A high resolution profiling ADV (Nortek Vectrino Profiler) sampled three components of velocity at 64 Hz with a 1 mm resolution over a 3 cm range intersecting the bed. The profiling ADV provided measurements of bed elevation, with sub-millimeter resolution. Additionally, an acoustic Doppler current profiler (Nortek Aquadopp High Resolution ADCP) was deployed only during the summer storm and used for high resolution velocity estimates over an 80 cm profile sampled at 1 Hz. An Imagenex 881A two-axis rotating sonar measured the bed profile with cm scale resolution over 2 m range and was used to qualitatively assess occurrences of suspended sediment (from backscatter intensity profiles).

2.3. Erosion chamber experiments

A modified EROMES erosion chamber (Tolhurst et al., 2000; Kalnejais et al., 2007) was used during all erosion experiments to quantify nutrient release from sediment due to resuspension induced by shear stress (Fig. 3b). The chamber uses an impeller and baffles within the core barrel to impose a shear stress at the sediment-water-interface. The chamber was previously calibrated for shear stress using a Shields Curve calibration (Kalnejais et al., 2007). Sediment cores for the erosion chamber experiments were collected from two locations in the Great Bay, selected to span the length of the Great Bay and to fall within the dominant sediment type found in the Bay. The first site at Jackson Estuarine Research Laboratory (JEL) is a previously established field site 100 m from the instrument array in an adjacent embayment and 1.5 m water depth at low tide (Fig. 1). The second site is in the middle of the Great Bay near the Squamscott River outlet (SQM) in 3.5 m water depth at low tide. All cores were collected with manual piston coring. Cores were discarded if there was any evidence of disturbance. SQM cores were placed on ice immediately after collection and transported to the Jackson Estuarine Lab where they were placed in a 4 °C refrigerator until the erosion experiments could be started. The JEL cores were carried immediately into the refrigerator. All experiments were performed within 2 h of core collection, except for SQM core 2, which could only be measured 17 h after collection. Duplicate erosion experiments were performed at JEL in spring (3 June 2011, experiments JEL-J1 and JEL-J2) and summer (4 August 2011, experiments JEL-A1 and JEL-A2), and once at SQM in summer (16 August 2011, experiments SQM-A1 and SQM-A2). Associated with each erosion experiment, additional cores were collected and sectioned to provide porewater profiles and the underlying sediment geochemistry at each site (Percuoco et al., 2015).

Nutrient release was estimated with erosion experiments following the protocol detailed in Kalnejais et al. (2010). Briefly, the shear stress imposed on the core was incrementally increased, and water samples for nutrient and total suspended solid analysis were collected from the overlying water 15 min after the shear stress change. Water removed due to sampling was replaced with estuarine water to maintain a constant chamber volume. All erosion results are corrected for the water removed during sampling. Shear stresses in the range 0–0.4 N m^{-2} were imposed. To accommodate simultaneous determination of turbidity during JEL-A2, SQM-A1 and SQM-A2 experiments, the EROMES chamber was connected to

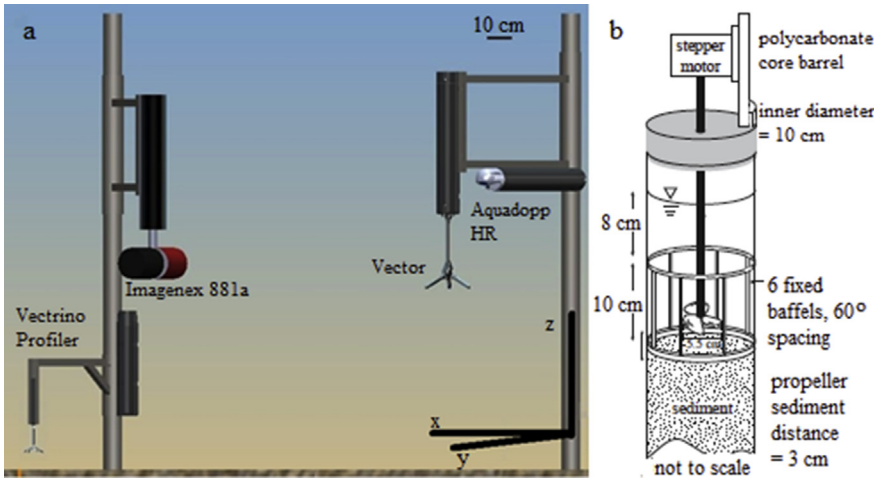

Fig. 3. (a) Hydrodynamic field instrument array showing instrument locations relative to the bed. Instrument poles are at the same across channel location but were offset in the along channel direction by 8 m. The x-axis is in the along channel direction (positive south), the y-axis is in the across channel direction (positive east), and the z-axis is positive up. (b) Laboratory based EROMES erosion chamber (from Kalnejais et al., 2007).

an additional chamber. The additional chamber increased the total volume from 1.7 to 3.5 L. Overlying water was circulated between the chambers with a peristaltic pump, and the turbidity chamber was mixed with a magnetic stirrer. For select experiments, several shear stress steps (JEL-A1 0.16 Nm^{-2}, SQM-A2 all shear stress > 0.17 Nm^{-2}) were held for longer than 15 min. The nutrient concentrations were monitored over the longer shear stress steps (that lasted up to 45 min) and typically did not change by more than 10% (Percuoco et al., 2015), so only the 15 min data is discussed here. To normalize for the volume variations between experiments, all solute data is reported as nutrient release N_n (mmol/m^2) at the n-th shear stress step:

$$N_n = (C_n - C_o) \times \frac{V_{total}}{A_{chamber}} \quad (1)$$

where C_n is the concentration measured at the n-th shear stress step. C_o is the initial nutrient concentration, V_{total} is the total volume of water used in the erosion experiment and $A_{chamber}$ is the sediment area in the erosion chamber.

As with all sampling methods, the laboratory based erosion experiments have drawbacks that limit application to natural systems; these include non-uniform shear stresses imposed across the sediment–water interface of erosion chambers that vary depending on the type of device (Gust and Muller, 1997), and the small footprint of the chambers make it difficult to resolve any potential heterogeneity in the estuarine surficial sediment.

2.4. Nutrient analysis

All water samples were immediately filtered with a 0.45 μm polycarbonate filter membrane and refrigerated immediately. All analysis was completed within three days of core collection. Nutrients were analyzed colorimetrically. Ammonium and phosphate were determined using the method of Strickland and Parsons (1968). Nitrate + nitrite was determined spectrophotometrically with the method Zhang and Fisher (2006) using an acidified resorcinol reagent. Both species are referred to further as nitrate. The protocol of Zhang and Fischer (2006) was modified slightly as excess HCl (125 μL of 4 M HCl for 1 ml sample) was added to ensure the chloride ion concentrations was adequate to catalyze the reaction in estuarine water samples. Standard additions experiments were performed at least once per chamber experiment to verify the nitrate protocol. The samples were quantified with a Perkin Elmer Lambda 600 UV–VIS spectrophotometer with detection limits of 0.1 μM for ammonium and phosphate and 0.2 μM for nitrate.

Porosity was determined on a separate core that was collected at the same time. The suspended sediment concentration was determined gravimetrically and used with the porosity to estimate erosion depth (Kalnejais et al., 2007).

2.5. Data collection

Field observations were obtained during two deployments, each with similar tidal range but with the first during mild winds (June

Table 1
Sediment grain size distribution and classification for the Adams Point sampling site and theoretical reference cases.

Sediment type	Mud	Fine sand	Medium sand	Sand	Shepard classification
Standard grain size upper limit[a]	65 μm	250 μm	1 mm	2 mm	–
Adams Point sampling site	25%	62%	13%	–	Muddy-sand
SQM Sampling Site	54%	44%	2%	–	Sandy-mud
JEL Sampling Site	60%	38%	1%	–	Sandy-mud
Reference sediment classification	>75%		<25%		Mud
distribution limits[b]	>50%		<50%		Sandy-mud
	>25%		<75%		Muddy-sand
	<25%		>75%		Sand

[a] (USGS, 2005).
[b] (Shepard, 1954).

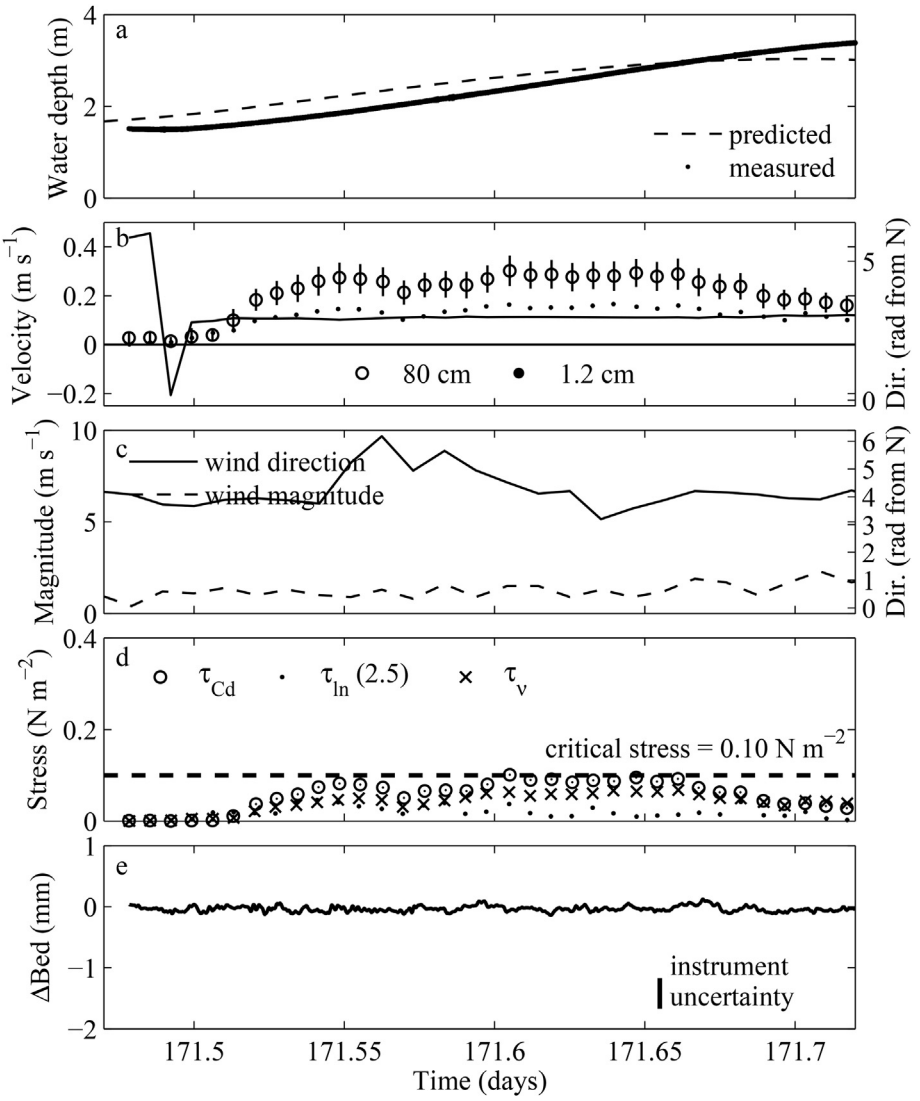

Fig. 4. Non-storm condition hydrodynamic, wind, and bed elevation observations. (a) Tidal level at Adams Point. (b) Temporally averaged velocity ± one standard deviation for the ADV (open circle), temporally and spatially averaged velocity ± one standard deviation for the profiling ADV (black dot), and current direction as calculated from ADV (black line). (c) Wind magnitude and the direction from which the wind is blowing (in radians clockwise from true North) observed from the Great Bay Coastal Buoy. (d) Bed stress estimated with: a quadratic drag law (ADV), log model (profiling ADV), and viscous sublayer (profiling ADV). The dashed line indicates the critical stress (0.10 N m^{-2}). (e) Change in bed elevation estimated with the profiling ADV.

2011) and the second during higher winds associated with Tropical Storm Irene (August 2011). For the first deployment, winds were light and variable with speeds less than 1.5 m s^{-1}. For the second deployment, Hurricane Irene made landfall 300 km south of the field site and traveled inland gradually losing energy overland, eventually being downgraded to tropical storm status. The winds at the deployment site (up to 8 m s^{-1}) were significantly higher than before, but moderately low for a tropical storm event. Two days prior to the tropical storm, three sediment cores were collected as close as possible (within 10 m) to the instrument array at the Adams Point site, two for erosion chamber experiments (denoted Irene1 and Irene2) and one for determining porosity. The erosion experiments on these cores were compared to *in situ* observations during Tropical Storm Irene, and used to assess the performance of the erosion chamber. Bay water samples were collected every 1–4 h 100 m adjacent to the instrument array to provide data on salinity and total suspended solids in the water column during the storm.

2.6. Determination of bed shear stress and erosion thresholds

Conditions for rough turbulent flow (when the boundary roughness elements are of similar magnitude to the viscous sublayer) and threshold for incipient motion of sediment (when the destabilizing force applied by the boundary layer exceeds the resistive forces of the sediment grains) both rely on accurate estimates of the shear stress (τ). As no direct measurement of the shear stress is possible, proxy methods have been developed for tidal boundary layers (Gross and Nowell, 1983; Kim et al., 2000). In this effort, three methods are considered. First, the bed stress, is roughly approximated with a quadratic shear stress law given by,

$$\tau_{Cd} = \rho C_d U^2 \tag{2}$$

where ρ is the density of the fluid, C_d is a drag coefficient, and U is the free stream velocity (Soulsby, 1997). The free stream velocity is taken as the 20 min average horizontal velocity measured by the ADV

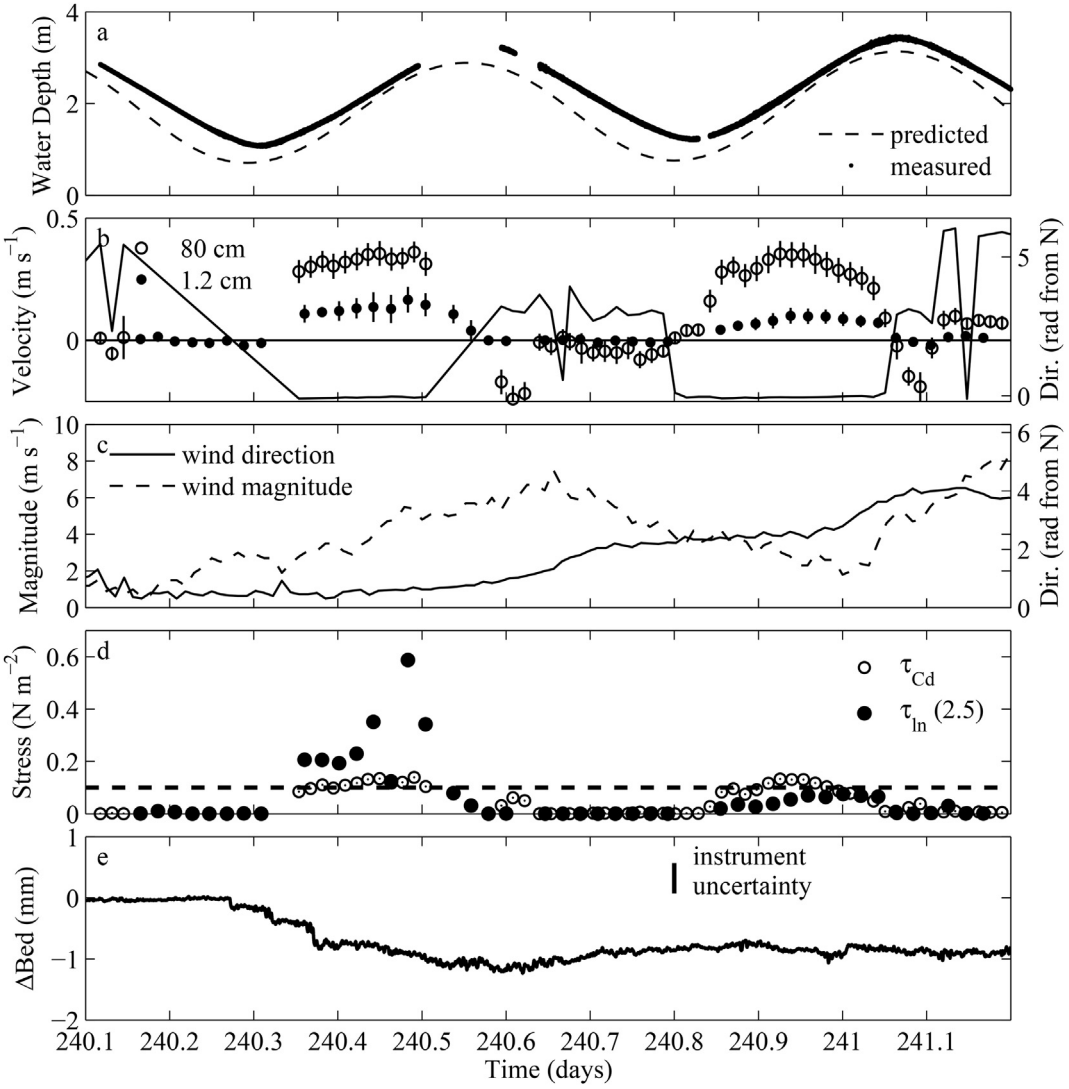

Fig. 5. Storm condition hydrodynamic, wind, and bed elevation observations. (a) Tidal level at Adams Point. (b) Temporally averaged velocity ± one standard deviation for the ADV (open circle); temporally and spatially averaged velocity ± one standard deviation for the profiling ADV (black square); and current direction from the ADV (black line). (c) Wind magnitude and the direction from which the wind is blowing (in radians clockwise from true North) observed from the Great Bay Coastal Buoy. (d) Bed stress estimated with: a quadratic drag law (ADV) and log model (profiling ADV). The dashed line indicates the critical stress (0.10 N m^{-2}). (e) Change in bed elevation estimated from the profiling ADV.

70 cm above the bed. The drag coefficient ($C_d = 0.001$) was estimated as an average of the Dawson-Johns, Soulsby, full depth log profile, and Colebrook–White methods following Soulsby (1997).

In the fully turbulent flow regime, bed stress ($\tau_{ln} = \rho u_{*ln}^2$) is approximated by assuming a logarithmic boundary layer model. The shear velocity, u_{*ln}, is one of two free parameters determined with the vertical profiles of the horizontal velocities, $u(z)$, measured with the profiling ADV observations (Tennekes and Lumley, 1972), given by,

$$u(z) = \frac{u_{*ln}}{\kappa} \ln\left(\frac{z}{z_0}\right) \tag{3}$$

where κ is the von Karman coefficient (estimated to be 0.4), z is the distance from the boundary, and z_0 is the roughness length. The shear velocity can be estimated with the indicator function method by taking the derivative of Eq. (3) with respect to z (Orlü et al., 2010). This technique has been shown to give a robust estimate of u_* while removing consideration of the second free parameter z_0 (Tennekes and Lumley, 1972; Orlü et al., 2010; Wengrove and Foster, 2014).

In laminar or smooth turbulent flow, when the nearbed turbulent contributions are small, the stress is assumed to be equivalent to the viscous stress, τ_v, and can be estimated at any elevation within the water column (Davidson, 2004),

$$\tau_v = \mu \frac{\partial u}{\partial z} \tag{4}$$

where μ is the dynamic viscosity. In the viscous sublayer, where the viscous forces dominate the turbulent contributions, the bed stress results from molecular momentum transfer (Boudreau and Jorgensen, 2001). In this effort when there is evidence of a viscous sublayer, the viscous stress is estimated using data from the profiling ADV that can resolve very near bed velocity profiles. Additional information is provided in Wengrove and Foster (2014).

3. Results

3.1. Physical observations

The hydrodynamic sampling array was located in the shallows of the main channel of the Bay (Fig. 1 A), where channel orientation is north-south and the flooding tide flows to the south. The

incoming flow indicates unidirectional flow parallel to the channel during flood tide for both deployments (Figs. 4b and 5b, where a flow direction of 0 radians is due south). During ebb tide, topographic sheltering from a small peninsula to the south of the sampling site directs the outgoing flow away from the shallow mud flats and into the deeper main channel, creating very low velocity magnitudes at the instrument location (nearly 0 m s^{-1}; see Fig. 5b). Consequently, this paper focuses on the flood phase of the tide for both non-storm and storm conditions.

Free stream and near-bed velocities observed during both the non-storm (Fig. 4) and storm (Fig. 5) deployments show that horizontal velocities remain relatively uniform over the mid flooding tide. The local velocity magnitude during mid-flood tide was 0.28 m s^{-1} during non-storm conditions and 0.35 m s^{-1} during Tropical Storm Irene. Energy density spectra of the near bed and free stream velocity data show no evidence of energy in the free surface gravity band (not shown); therefore, wave energy is assumed to be attenuated and hydrodynamic forcing is assumed to be dominated by the mean tidal currents.

Observations from the two ADVs allowed for several independent estimates of the bed stress (Figs. 4d and 5d; where a dashed line represents the critical stress τ_c). During non-storm conditions all three estimates of stress are in agreement and indicate that the incipient motion threshold was approached but not surpassed (Fig. 4d). Changes in bed elevation relative to the beginning of the given sampling windows (Figs. 4e and 5e) show that for the non-storm condition there is no overall change in bed elevation, while during the storm condition the bed elevation decreased by 1.2 mm beginning at day of year (DOY) 240.25. Please note, that an examination of the hydrodynamic regime with the roughness Reynolds number, Re_* (<3.5), indicates the bed roughness is smaller than the laminar boundary layer thickness and is consistent with smooth turbulent flow with a viscous sublayer several millimeters thick (this was supported with a supplementary investigation of the velocity profile within the lowest 1 cm by Wengrove and Foster (2014)). Ancillary support for the smooth turbulent flow assumption during the non-storm conditions was provided by the presence of an immobile bed (Figs. 4e) and $\tau < \tau_c$.

Under storm conditions, the threshold for incipient motion was surpassed during the first flood tide (DOY 240.30–240.55; Fig. 5d). Erosion of the bed exceeded 1.2 mm (Fig. 5e) and the duration of erosion and initiation of erosion are concurrent with estimates of bed stress exceeding the critical threshold (Fig. 5d,e DOY 240.30–240.55). Consequently, no estimate for the viscous stress is included. There is considerable variability between the two stress estimates once the threshold of incipient motion is reached. A possible explanation for the discrepancy is an underestimate of the drag coefficient once the no slip condition has failed.

3.2. Comparison of field observations with erosion chamber data

The variation of measured bed elevation as a function of bed stress for both non-storm and storm conditions in comparison with erosion chamber data (sediment cores, Irene1 and Irene2) is shown in Fig. 6. For each erosion experiment, initial increases in shear stress did not lead to erosion. The critical shear stress calculated from erosion chamber experiments is 0.11 ± 0.1 N m^{-2} (determined by a linear regression of total suspended solids as a function of shear stress following the method of Amos et al., 2003). Beyond the erosion threshold, the suspended solids concentration increased with increasing shear stress. The calculated erosion depth corresponding to each stress level is shown in Fig. 6. The calculated erosion depths for both cores agree (within error limitations) up until a shear stress of 0.17 N m^{-2}. At higher shear stresses the erosion depths diverge, with core Irene1 consistently eroding

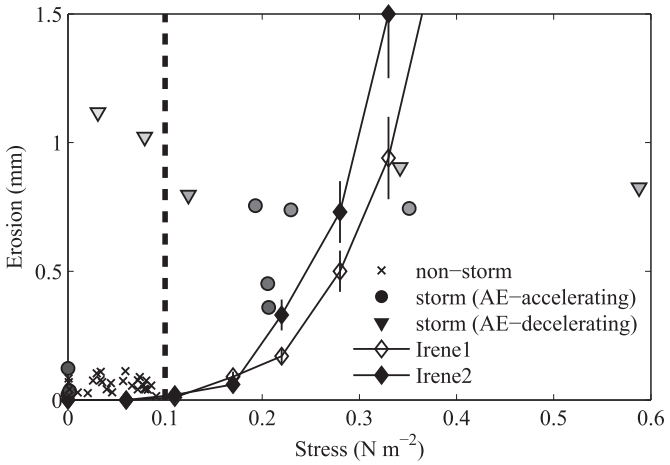

Fig. 6. The logarithmic estimate of bed stress related to erosion depth for *in situ* (non-storm, storm) and erosion chamber experiments. Cores Irene1 and Irene2 are duplicate cores sampled one day before Tropical Storm Irene arrived. The error in the calculated erosion depth from the erosion chamber is propagated from the variability in porosity data (Kalnejais et al., 2007). For the *in situ* experiment, all non-storm flood tide data is shown, while for the storm event, only data from the first flood tide (where there was active erosion (AE) of the bed) is shown. The *in situ* data is plotted with shading gradation from dark (low tide) to light (high tide) as the flood tide progresses, where circles represent the accelerating flood tide (AE-accelerating) and triangles represent the decelerating flood tide (AE-decelerating). The dashed line indicates critical stress (0.10 N m^{-2}) determined from the field data for incipient motion, the incipient motion as measured in the EROMES erosion experiment is 0.11 N m^{-2}.

slightly more sediment than core Irene2. At a shear stress of 0.33 N m^{-2}, core Irene1 and core Irene2 eroded to a depth of 1.5 ± 0.2 mm and 0.9 ± 0.2 mm, respectively.

Periods of increasing stress during the storm, when erosion was actively occurring are compared with the erosion chamber results because this best represents how the erosion chamber operates (with successively increasing shear stress steps) (Fig. 6). This comparison excludes field observations when deposition was occurring, a condition that the erosion chamber did not simulate. There were periods when the erosion depth was increasing, but the time averaged shear stress remained constant (e.g. DOY 240.35–240.4). To differentiate between multiple observations of erosion depth at the same shear stress, the field observations in Fig. 6 are plotted with shading gradation from dark to light as the active erosion flood tide progresses from low tide (dark) to high tide (light), where circles represent acceleration of flow (DOY 240.30–240.45) and triangles represent deceleration of flow (DOY 240.45–240.60).

The erosion threshold measured by the erosion chamber (0.11 ± 0.1 N m^{-2}) compares well with the observed field critical shear stress for incipient motion of 0.10 N m^{-2}. Once the threshold for incipient motion is reached, the erosion depth curve in the chamber is similar to the erosion signature observed in the field up to 0.75 mm of erosion and a shear stress of 0.35 N m^{-2}. Beyond a stress of 0.35 N m^{-2}, the erosion chamber continues to erode (with both cores eroding to a depth of 2.2 ± 0.4 mm by 0.39 N m^{-2}), whereas the field data show an erosion depth of 0.8 mm at the peak shear stress of 0.58 N m^{-2}.

3.3. Nutrient release due to resuspension

The nutrient release associated with resuspension at two sites representative of the dominant sandy-mud regions of the Bay (Table 1) was determined 1–3 weeks prior to Tropical Storm Irene. These results will be used to provide an estimate of nutrient release

during the storm, and are discussed below. An additional spring data set is also included to provide information on the temporal variability of nutrient release. The effect of erosion on the release of ammonium, nitrate and phosphate at the JEL and SQM sites is shown in Fig. 7. There was limited ammonium release until the erosion threshold was exceeded in five of the six cores. Only core JEL-J1, had an ammonium release before the erosion threshold. Beyond the erosion threshold, the ammonium release increased with shear stress for all cores. The only exception to this was JEL-A2 which showed a decrease in ammonium release at 0.27 Nm^{-2}, however there was a leak in the chamber at this shear stress step, so the solute release presented for the final three shear stress steps in the JEL-A2 data represents a lower bound for the release as an uncertain volume of fluid was lost from the chamber. The erosion chamber data is from two sites and from two different seasons, yet the ammonium release is relatively consistent, with an average ammonium release of 0.9 ± 0.3 mmol m^{-2} at a shear stress of 0.35 Nm^{-2} (mean ± standard deviation for n = 5, the data from JEL-A2 is excluded due to the leak).

The phosphate release as a function of shear stress is less consistent than the ammonium data. For example, there is considerable variability between seasons at the JEL site. In the summer phosphate was released by sediment bed erosion, whereas in spring no significant release with increasing stress was observed (Fig. 7b). For the summer data at both JEL and SQM, there was no significant change in phosphate release until after the erosion threshold was exceeded. In three cores (JEL-A1, JEL-A2 and SQM-A2) there was a net release of phosphate after the erosion threshold, however the release was not monotonic with increasing shear stress, indicating removal of phosphate was also occurring. For example, a very strong phosphate removal occurred at a shear stress of 0.39 Nm^{-2} in the JEL-A1 experiment, where the phosphate release decreased by more than 40% relative to the previous shear stress. The fourth summer core, SQM-A2 behaved differently and showed a net removal of phosphate, with the removal increasing with increasing shear stress.

There was typically a net release of nitrate after the erosion threshold. The only exception to this was SQM-A1, which shows a net removal of nitrate. For this core, the nitrate removal occurred at the first shear stress step and then remained fairly constant over the remainder of the experiment. SQM-A2 also showed evidence of nitrate removal prior to the erosion threshold, however in this core subsequent release of nitrate beyond the erosion threshold counteracted the initial removal, and there was a net release for shear stresses above 0.27 Nm^{-2}. The nitrate release, like the phosphate release was also not monotonic with shear stress, so there is also evidence of nitrate removal during resuspension. The average nitrate release at 0.35 N m^{-2} was 0.3 ± 0.4 mmol m^{-2} (n = 5), with

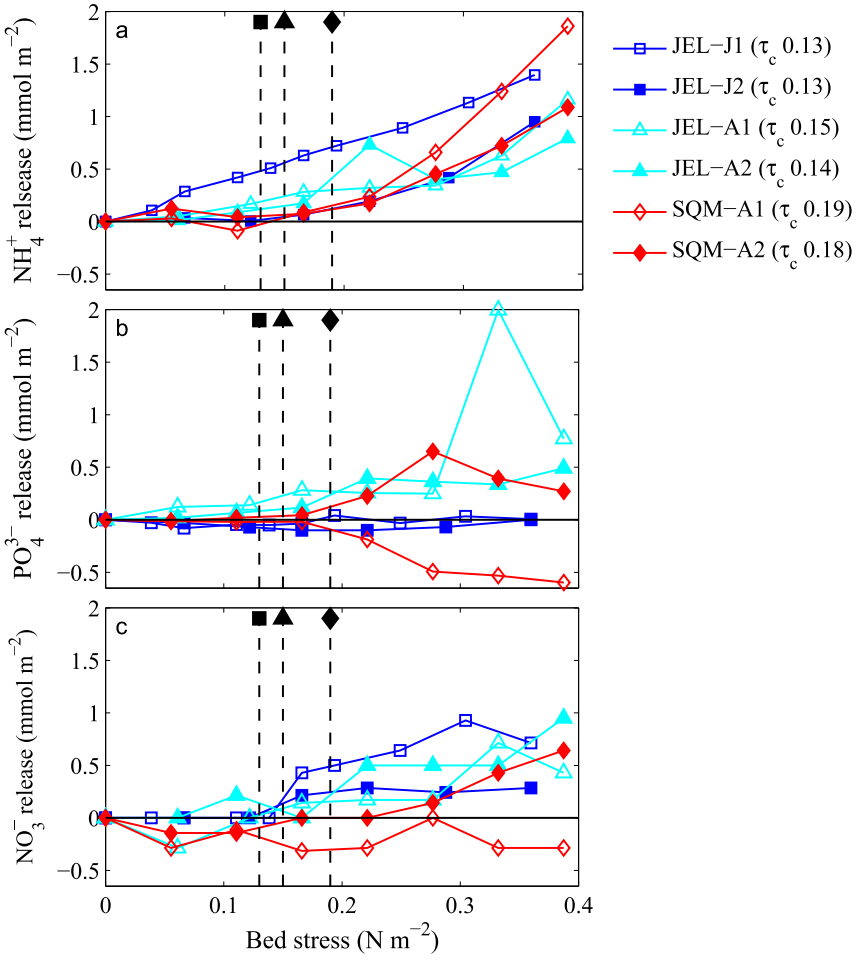

Fig. 7. Ammonium (a), phosphate (b), and nitrate (c) release measured in the erosion chamber as a function of applied bed stress from JEL and SQM sites. Duplicate erosion experiments were performed at each site Erosion thresholds (Percuoco et al., 2015) for each experiment are provided next to the legend and plotted on the figure as a vertical dashed line with respective symbol in black near the top of each panel. Nutrient release is given in mmol m^{-2} to normalize for different chamber volumes. The measured concentration range (μM) during the erosion experiments for the duplicate experiments at each site were: JEL-J (ammonium 5.1–9.4, phosphate 0.2–0.8, nitrate 4.5–6.2), JEL-A (ammonium 1.8–6.6, phosphate 1.5–10.9, nitrate 0.2–3.3) and SQM (3.0–7.2, phosphate 0.3–2.1 (core 1) 1.4–2.7 (core 2), nitrate 2–4.9). The final three points from the JEL-A2 experiment represent minimum release values, as a leak developed in the chamber.

the large variability predominantly driven by the single core that demonstrated removal. The average release of dissolved inorganic nitrogen (DIN = nitrate + ammonium) at 0.35 Nm^{-2} was also relatively consistent between sites and seasons, at 1.2 ± 0.4 mmol m^{-2} (n = 5), because ammonium release dominated the DIN behavior.

4. Discussion

4.1. Non-storm vs. storm conditions

Observations from non-storm conditions showed that the bed is immobile and the flow field has a viscous sublayer that is larger than the roughness length (see Wengrove and Foster (2014) for further discussion of methods for calculating the viscous sublayer properties). This would support the assumption of molecular diffusion of nutrients from sediment porewaters, commonly used to quantify fluxes from sediments. Periods of sediment mobility during the storm deployment coincide with the flooding tide and are in the same direction as the winds (aligned by topographic channeling through the Bay; Figs. 4 and 5).

During the storm, rainfall (not shown) remained low and the measured salinity at the sampling location did not significantly change, indicating that river flows did not significantly influence this site. The wind is the likely cause of the 20% higher free stream velocities at the shallow field site, leading to sediment resuspension and just over 1 mm of bed erosion. Given that the threshold for incipient motion was surpassed, the boundary layer is considered to be fully turbulent and for this range of stresses the logarithmic boundary layer was expected to reach the bed. In this case, nutrient release is considered be enhanced by both the presence of turbulent diffusion and also due to the suspension of sediment and accompanying porewater.

During non-storm conditions all estimates of stress remain below the critical threshold, and the bed is stable to within the tolerance of the instrument. The presence of a viscous sublayer is consistent with expected theory and prevents the logarithmic boundary layer from reaching the sediment–water interface, and thus the viscous stresses were the dominant contribution to the total stress (Wengrove and Foster, 2014). When the smooth turbulent flow conditions were satisfied, the viscous stress (Eq. (4)) was estimated and is used for analysis presented in Figs. 6 and 8.

During storm conditions when the critical threshold for rough turbulent flow and incipient motion thresholds are exceeded, there are significant differences between the two bed stress estimates. The logarithmic estimate of the bed stress from the profiling ADV (τ_{ln} 2.5) is assumed to be the most reliable. The profiling ADV had a high near-bed resolution, and the skill (defined by the square of the correlation) of the logarithmic model fit to the velocity profile ranged from 0.87 to 0.95. Thus, during the storm condition the boundary layer is assumed to be fully logarithmic, further supported by the consistency between the τ_{ln} 2.5 stress estimate and the temporal change in measured bed response. During the flooding tide of the storm condition, the stress (τ_{ln} 2.5) exceeds the critical threshold while the sediment is actively eroding (see the active erosion phase of the first flood tide of the storm deployment; DOY 240.3–240.55), and shows smaller estimates of bed stress when the bed is no longer eroding (see the second flood tide of the storm deployment; DOY 240.8–241). The quadratic stress (τ_{Cd}) estimation was made with a single point measurement of velocity, and the lower magnitude τ_{Cd} could be indicative of an underestimate of the drag coefficient once the slip condition is exceeded.

Wind forcing in combination with the flood tide is the presumed source for enhanced bed stress that exceeded the threshold for sediment motion (Fig. 8a). The calculated bed stress from the profiling ADV is compared to the concurrent wind speed during the non-storm and storm deployments, and are separated into three subsets: 1) all flood tide data (includes periods of active and inactive erosion data), 2) only periods of active erosion data, and 3) ebb tide data. Both non-storm and storm conditions show that, at this site, when wind speeds are below 2 m s^{-1}, shear stress is less than 0.10 N m^{-2}, and the threshold for incipient motion is not exceeded (Fig. 4c,d and 5c,d). During the storm deployment (Fig. 5e, between DOY 240.2 and 240.6), it is apparent that the bed is actively eroding, the stress is above the critical threshold (Fig. 5d), and the wind acting is in the same direction as tidal current (Figs. 5b,c). When the wind and tidal current are acting in the same direction, the shear stress exceeds the threshold for incipient motion. Fig. 5 shows two measured flooding tides during Tropical Storm Irene. Wind magnitude and direction (Fig. 5c), where 0 radians indicates the wind is coming from the north (blowing towards south), coinciding with the dominant direction of tidal current during flood tide (flowing towards the south, Fig. 5b). During the first flood tide wind speeds ranged between 2 and 6 m s^{-1} and were generally blowing towards the south, aligning with the flood tide. During the

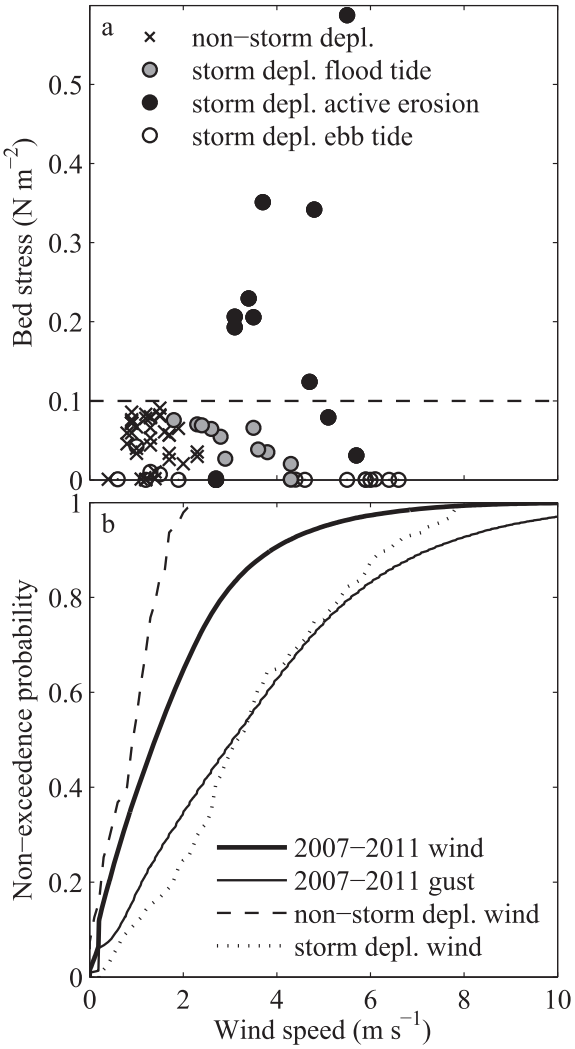

Fig. 8. Analysis of applied bed stress and associated physical wind forcing. (a) Bed stress related to wind speed for both non-storm and storm conditions. Dashed line indicates critical stress determined from the critical threshold for incipient motion. Where the active erosion flood tide (DOY 240.30–240.55 in Fig. 5) is a subset of the flood tide during the storm condition (DOY 240.30–240.55 and DOY 240.80–241.05 in Fig. 5). (b) Cumulative distribution of wind speed for both deployments (depl.) and a data set of hourly averaged wind speeds and gust speeds from 2007 to 2011.

subsequent flood tide the wind magnitude reached 8 m s^{-1}; however, the wind and current direction were opposing, and the bed stress did not reach critical level. During ebb tide the wind speed was, at times, greater than the wind speed during flood tide; however, the tidal current and the wind were acting in different directions (Fig. 5d) resulting in lower bed stress.

For active erosion to persist, the tidal and wind-driven currents must be in the same direction. Given the limited duration of the two deployments, an evaluation of the fraction of time (or likelihood) these conditions are satisfied requires other longer term observations. Winds can be used as a rough proxy for examining the probability of exceedance of storm conditions. A cumulative distribution of wind and gust speed for both deployments is shown in Fig. 8b, along with average wind speed and wind gust data for 2007 through 2011 (CICEET, 2011). The wind speed distribution during the non-storm deployment was lower than the average wind speed distribution for the 2007 through 2011 record, and the wind speed during the storm deployment represents a short window where sustained wind speeds are comparable to the five year cumulative distribution of wind gusts. Although wind speeds during the Tropical Storm Irene deployment are not extreme, they provide an example of how sustained wind forcing can enhance the water column flow field that can lead to sediment mobilization.

The combination of wind driven flows and tidal currents could significantly affect the long term erosive nutrient release to the estuarine system. Wind speed during the sampled non-storm deployment was generally 2 m s^{-1} or less, which is approximately equal to the wind speed that occurred 75% of the time between years 2007–2011. The storm deployment had periods of active sediment erosion correlated with wind speeds 3 m s^{-1} or greater, and had distribution approximately equal to that of the gust speed for data between 2007 and 2011 (Fig. 8b). The average wind speed between 2007 and 2011 is greater than 3 m s^{-1} approximately 15% of the time, providing an upper bound to the probability of erosive conditions.

4.2. Observations of erosion and accuracy of the erosion chamber

The erosion chamber data follow a trend of increasing erosion depth with increased bed stress (Fig. 6). This pattern is different than the erosion pattern seen in the field during active erosion storm conditions, where almost 70% of the erosion occurs during the accelerating phase of the flood tide when the stress was increasing. During the decelerating phase of the flood tide erosion when the stress was declining but still larger than the critical threshold, rates begin to decrease even though there is an instance of high applied stress. This difference in behavior could be due to variability in the storm pattern creating high effective stress but with durations too short to erode sediment (compared to the continuous forcing imposed in the erosion chamber). However, an equally likely explanation is sediment heterogeneity and depth varying heterogeneity, such as armoring at the instrument array but not in the erosion chamber (Sanford and Maa, 2001; Tolhurst et al., 2009). Changes in sediment composition over depth are not known at the sampling location, but could be significant.

The field data agree with the erosion chamber measurements at lower stresses up to 0.35 N m^{-2} (Fig. 6). Low shear stresses occur more frequently, so the erosion chamber appears to be well suited to represent a significant proportion of erosion events. The EROMES chamber did not simulate a cessation of erosion beyond a shear stress of 0.35 N m^{-2}, as was observed in the field (Fig. 6). The trend measured by the EROMES chamber is consistent with other erosion experiments (Gust and Muller, 1997; Dewhurst et al., 2000; Couceiro et al., 2013). Further experiments and observations are required to determine reasons for the discrepancy at high shear stress.

4.3. Nutrient release due to resuspension

Results show that dissolved inorganic nitrogen release is determined largely by flow conditions that exceed critical shear stress values for fine-grained sediment, suggesting that turbulent release is important to the overall nutrient budget in the estuary during tidal plus wind forcing conditions. The close agreement between the field data and the EROMES erosion chamber up to a shear stress of 0.35 N m^{-2}, suggest the dynamics of resuspension are well simulated in the chamber.

The increasing release of ammonium with increasing shear stress (Fig. 7a) was also reported by Kalnejais et al. (2010) for Boston Harbor, and attributed to the increasing entrainment of porewaters and the likely desorption of ammonium from resuspended particles. One of the cores (core JEL-J1) shows ammonium release before the erosion threshold is exceeded. The mobilization of a fluff layer before bulk sediment resuspension begins may account for this release (Couceiro et al., 2013). This release prior to the erosion threshold increases the magnitude of the ammonium release during an erosion experiment, however it was only observed in a single core, so a fluff layer does not seem to be a persistent feature in the Great Bay. The release of nitrate due to resuspension was observed in all cores except SQM-A1, and may be due to the stimulation of nitrification by the turbulent conditions (Couceiro et al., 2013). Nitrate removal is also observed at several shear stresses in multiple cores, including before the erosion threshold. The processes removing nitrate are unclear, but could be due to nutrient uptake by benthic primary producers, stimulated by the enhanced flow rates imposed by the erosion experiment, or adsorption to particles. While these processes likely also impact ammonium release, the release of nitrate during resuspension may not be as consistent, so in some cases removal dominates the nitrate response.

The role of sediment resuspension in phosphate cycling remains poorly defined. Several studies have shown sediment resuspension is a source of phosphate to marine waters (Kalnejais et al., 2010; Couceiro et al., 2013), while others have shown no effect (Almroth et al., 2009) or a removal of phosphate from the water (Tengberg et al., 2003). This data shows that the influence of sediment resuspension on phosphate release can also change seasonally and with high spatial variability. Although there was no phosphate release during resuspension at JEL in spring, measurements on cores collected at the same time as the erosion cores, showed there was phosphate in surface porewaters (0–3 mm depth interval) (Percuoco et al., 2015). Porewater phosphate was thus entrained into the overlying water of the chamber during erosion, but there was likely no overall release of phosphate during spring at the JEL site because it was completely removed from the water column by scavenging. Iron (oxy)hydroxides are powerful scavengers of phosphate (Sundby et al., 1986) and will be freshly formed in the water column as iron(II) from the sediments is entrained and oxidized in the water column. The average iron concentration in the surface porewaters at JEL in spring was 230 ± 130 μM compared to 34 ± 30 μM in the summer, and the porewater Fe : PO_4^{3-} ratio was 34 ± 5 in spring and 9 ± 2 in summer (Percuoco et al., 2015). The greater abundance of iron relative to phosphate may account for the absence of any phosphate release during resuspension in spring. The controls on phosphate release require further investigation as the two SQM experiments have an opposite phosphate response that cannot be fully explained by the available iron data. The SQM porewater iron (80 ± 60 μM) and Fe : PO_4^{3-} ratio (11 ± 5) were closer to the summer JEL values (Percuoco et al., 2015), so phosphate release would be predicted based on the JEL response. The Fe : PO_4^{3-} ratio at the SQM site was more variable than at JEL, and this may have

been responsible for the variable erosion chamber response. The half-life for phosphate with respect to iron oxyhydroxide scavenging is less than 15 min (Crosby et al., 1984), so the sampling interval used in this study (15 min) only provides information on the water chemistry after significant scavenging has already occurred. Future work should include determinations of iron speciation and phosphate at higher frequency in the erosion chamber to provide more detailed information on the formation of iron oxyhydroxides and subsequent phosphate scavenging over time.

4.4. Sediment resuspension and first order approximation of nutrient budget

To provide a preliminary estimate of the importance of sediment resuspension on the nutrient budget in the Great Bay, the temporally varying field estimates of shear stress during the storm can be coupled to the erosion chamber nutrient release measurements. Only nutrient release measurements corresponding to an applied stress of up to 0.35 N m^{-2} are included in this approximation, as beyond 0.35 N m^{-2} the erosion chamber and *in situ* erosion depth observations do not agree. The storm reached a peak shear stress of 0.58 N m^{-2} at Adams Point. Without records of shear stress during the storm at additional sites or a hydrodynamic model to predict the shear stress, we assume that at some time during the storm the muddy sediment in the Bay experienced a shear stress of at least 0.35 N m^{-2}. Considering that the AP site reached a higher shear stress, is at the same depth or deeper than most of the muddy sediments in the Bay, and is sheltered from high stresses during ebbing tide, it is likely that other muddy sites experienced at least 0.35 N m^{-2} at some stage of the tidal cycle while storm winds were present.

The average dissolved inorganic nitrogen and phosphate release measured in summer at JEL and SQM at a shear stress of 0.35 N m^{-2} was 1.3 and 0.21 mmol m^{-2}, respectively (excluding JEL-A2 data due to the leak and the large phosphate peak in core JEL-A1). To make a first order approximation of the influence of an event-based release on the estuarine system, the average summer nutrient release measured at these two representative sites is scaled up to a larger area of the Bay. Regions that are considered appropriate to apply the erosion chamber data include areas that have a high tide water depth of greater than 0.5 m (to constrain erosion processes to tidal currents and wind induced mixing) and areas that have the same or greater mud content (classified as sandy-mud or mud from Table 1) as the JEL and SQM sites.

The Great Bay system encompasses 22 km^2 of land area (excluding areas that have a shallower depth than 0.5 m at low tide). The sediment aerial distributions from Fig. 2b estimate that 58% of the system has sediment with 50% mud or more, while sediment distributions from Fig. 2c estimate that 55% of the Bay has sediment with 50% mud or more. If the more conservative estimate of 55% is used, then the summer erosion chamber data is taken to be representative of a 12 km^2 area of the Bay. With this estimate of area, the Bay-wide nutrient release associated with erosion up to 0.35 N m^{-2} can be approximated by assuming the average release from the erosion chamber applies to any site that experiences that shear stress for at least 15 min. With these assumptions, the nutrient release can be estimated with the following scaling approach:

$$\text{Nutrient Release(kg)} = \frac{N_{SS}}{1000} A_{sed} \frac{\text{AW}}{1000} \quad (5)$$

where N_{SS} is the average nutrient release for all shear stresses up to and including a particular cutoff shear stress (SS) (mmol m^{-2}) in this case the cutoff shear stress is 0.35 N m^{-2} and the average nutrient release is the summer nutrient release from Fig. 7, A_{sed} is the area of 50% mud sediment in the Bay (m^2) (~12 km^2 for this system) and AW is the atomic weight of nitrogen or phosphorus ($gmol^{-1}$). This rough calculation suggests that at a shear stress of 0.35 N m^{-2}, 220 kg of N (from dissolved inorganic nitrogen) and 80 kg of P (from phosphate) were released during the storm due to resuspension.

This first order approximation assumes that regions of the Bay that have a similar sediment type and depth also have sediments with similar geochemistry and erodibility. More robust estimates require additional erosion chamber experiments and field observations at multiple locations. The consistency of the ammonium and DIN erosion chamber data between sites and seasons gives confidence in the up-scaling of the DIN release, however assumption of similar chemistry may not be appropriate for phosphate, given the variability in phosphate response on a small spatial scale at SQM. *In situ* measurements during storms are required to definitively determine the impact of episodic events, but due to the considerable sampling infrastructure required to perform such measurements under intense wind and flow conditions, this first order estimate is valuable in assessing the potential impact of episodic events.

To compare these storm erosion releases to other nutrient sources in the Great Bay, previous estimates for the dissolved inorganic nitrogen loading and phosphorus loading are provided in Table 2. The riverine loads are at their lowest during the fall for both nutrients and a factor of 4–10 times higher in the spring (Table 2). The dissolved inorganic nitrogen released due to resuspension during Tropical Storm Irene is a small fraction (~10%) of the total summer monthly dissolved inorganic nitrogen load. The ammonium release increased with shear stress, so validating the erosion chamber operation beyond 0.35 N m^{-2} is important, as the total ammonium release may be higher due to the higher stresses that were reported. For phosphorus our rough estimate of storm release is 65% of the summer phosphorus monthly riverine loading and

Table 2
Load estimates from 5 rivers (Winnicut River, Bellamy River, Lamprey River, Squamscott River, Oyster River) that flow into the Great Bay and Little Bay.

Time frame	Dissolved inorganic nitrogen load (kg per month)	Phosphorus load (kg per month)	Data	Source
Winter (Dec.–Feb.)	3700	92	2000–2001	Oczkowski (2002) [b]
	7400	–	2009–2011	PREP (2012) [a]
Spring (Mar.–May)	17,000	720	2000–2001	Oczkowski (2002)
	15,000	–	2009–2011	PREP (2012) [a]
Summer (June–Aug.)	1300	120	2000–2001	Oczkowski (2002)
	3800	–	2009–2011	PREP (2012) [a]
Fall (Sept.–Nov.)	1200	70	2000–2001	Oczkowski (2002)
	4830	–	2009–2011	PREP (2012) [a]

[a] Trowbridge, P. PREP personal comm. updated from PREP (2012).
[b] Median values.

exceeds the fall phosphorus monthly riverine loading (the erosion chamber measurements and Tropical Storm Irene occurred at the end of summer, so may be representative of early fall conditions). This implies that this mild storm event could be a significant source of phosphate to the Great Bay. The phosphate erosive release is spatially variable throughout the Bay, so further work is required to understand the spatial extent of phosphate release and the chemical mechanisms determining the relative importance of release and adsorption of phosphate during resuspension. However, this preliminary data suggests that the phosphorus released from a 1 day resuspension event may be of the same order of magnitude as an entire month of riverine input. Resuspension is thus potentially important to the phosphate budget in the Bay.

An important aspect of this data set is that Tropical Storm Irene yielded wind speeds that were not extreme for this site (Fig. 8b), so resuspension events of a similar or greater magnitude are expected to occur multiple times per year in the estuary. The influence of sediment resuspension events on the nutrient budget of the Bay is dependent upon the number of events, and will have maximum effect on the nutrient supply when riverine nutrient inputs are low.

5. Conclusion

In this study, stress estimates and measured erosion depths from laboratory erosion chamber experiments were compared with field measurements. The erosion chamber and the *in situ* measurements both assess the threshold of incipient motion at the field site to be 0.10 N m^{-2}, which is consistent with the Shields estimate of critical stress. The erosion chamber and *in situ* measurements of erosion depth provide consistent results up to a bed stress of 0.35 N m^{-2} and an erosion depth of ~0.75 mm. These results suggest that the erosion chamber provides a reasonable simulation of the physical mechanisms occurring in nature within this stress range, providing confidence that the associated nutrient data is reliable.

To completely understand an estuarine ecosystem and to make informed decisions about watershed land use, coastal management, and influence upon water quality, it is necessary to consider nutrient loadings from all potentially large sources. This study shows that hydrodynamic forcing and consequent release of nutrients due to resuspension is important to consider when determining the nutrient input from estuarine sediment. The Great Bay, like many other estuarine ecosystems, is a large, shallow estuary dominated by tidal flows, so the effect of the local hydrodynamics on this depositional area is relevant to other estuarine systems (Dyer, 1973). During times when the critical threshold for motion is not exceeded, there is evidence of an observable viscous sublayer and the molecular diffusivity assumption is likely valid. As turbulence becomes dominant, the boundary layer becomes rough turbulent, and there are instances of sediment resuspension.

Erosive events rapidly release nutrients, and this preliminary assessment suggests that the quantity of phosphate released with resuspension events is a significant fraction of the loading from rivers at certain times of the year in the Great Bay estuary. Coastal systems worldwide have nutrients stored within their sediments that drive ecologically significant benthic nutrient fluxes under non-erosive conditions (e.g. Port Philip Bay, Australia (Berelson et al., 1998); Galveston Bay, USA (Warnken et al. 2000); Ragardsvic, Sweden (Sundbäck et al., 2003)). With climate change expected to intensify the magnitude and frequency of storms (Statham, 2012), increased erosion of fine-grained sediments is probable, and enhanced mobilization of the nutrients stored within these sediments is possible. Nutrient release due to sediment resuspension may already be a significant and generally unaccounted for term in the nutrient budget of shallow estuarine systems; considering future stressors, this nutrient source may become even more significant.

Acknowledgments

This work was supported by New Hampshire Sea Grant Project Number R/CE-141 and the University of New Hampshire's Departments of Earth Science and Mechanical Engineering. We also thank many University of New Hampshire Ocean Engineering and Earth Science students and alumni, whose brawn and brains made this field experiment a success. Two anonymous reviewers are thanked for their insightful comments that significantly improved this manuscript.

References

Almroth, E., Tengberg, A., Andersson, J.H., Pakhomova, S., Hall, P.O.J., 2009. Effects of resuspension on benthic fluxes of oxygen, nutrients, dissolved inorganic carbon, iron and manganese in the Gulf of Finland, Baltic Sea. Cont. Shelf Res. 29, 807–818.

Amos, C.L., Daborn, G.R., Christian, H.A., Atkinson, A., Robertson, A., 1992. In situ erosion measurements on fine-grained sediments from the Bay of Fundy. Mar. Geol. 108, 175–196.

Amos, C.L., Droppo, I.G., Gomez, E.A., Murphy, T.P., 2003. The stability of remediated bed in Hamilton Harbour. Lake Ontario, Canada. Sedimentology 50, 149–168.

Andersen, T.J., Fredsoe, J., Pejrup, M., 2007. In situ estimation of erosion and deposition thresholds by Acoustic Doppler Velocimeter (ADV). Estuar. Coast. Shelf Sci. 75, 327–336.

Berelson, W.M., Heggie, D., Longmore, A., Kilgore, T., Nicholson, G., Skyring, G., 1998. Benthic nutrient recycling in port Phillip Bay, Australia. Estuar. Coast. Shelf Sci. 46, 917–934.

Berelson, W., McManus, J., Coale, K., Johnson, K., Burdige, D., Kilgore, T., Colodner, D., Chavez, F., Kudela, R., Boucher, J., 2003. A time series of benthic flux measurements from Monterey Bay, CA. Cont. Shelf Res. 23, 457–481.

Bilgili, A., Proehl, J., Lynch, D., Smith, K., Swift, M., 2005. Estuary/ocean exchanged and tidal mixing in the gulf of Maine estuary: a Lagrangian modeling study. Estuar. Coast. Shelf Sci. 65, 607–624.

Boesch, D.F., 2002. Challenges and opportunities for science in reducing nutrient over-enrichment of coastal ecosystems. Estuaries 25, 886–900.

Boudreau, B., Jorgensen, B. (Eds.), 2001. The Benthic Boundary Layer. Oxford University Press.

Boynton, W.R., Kemp, W.M., 1985. Nutrient regeneration and oxygen consumption by sediments along an estuarine salinity gradient. Mar. Ecol. Prog. Ser. 23, 45–55.

CICEET, 2011. Great Bay Real-time Environmental Monitoring Network. Data. Cooperative Institute for Coastal and Estuarine Environmental Technology. URL: http://www.greatbaydata.org.

Crosby, S., Millward, G., Butler, E., Turner, D., Whitfield, M., 1984. Kinetics of phosphate adsorption by iron oxyhydroxides in aqueous systems. Estuar. Coast. Shelf Sci. 19, 257–270.

Couceiro, F., Fones, G., Thompson, C.L., Statham, P., Sivyer, D., Parker, R., Kelly-Gerreyn, B., Amos, C., 2013. Impact of resuspension of cohesive sediments at the Oyster Grounds (North Sea) on nutrient exchange across the sediment, Äiwater interface. Biogeochemistry 113, 1–16.

Cloern, J.E., 2001. Our evolving conceptual model of the coastal eutrophication problem. Mar. Ecol. Prog. Ser. 210, 223–253.

Cowan, J.L.W., Pennock, J.R., Boynton, W.R., 1996. Seasonal and interannual patters of sediment-water nutrient and oxygen fluxes in Mobile Bay, Alabama (USA): regulating factors and ecological significance. Mar. Ecol. Prog. Ser. 141, 229–245.

Davidson, P.A., 2004. Turbulence: a Introduction for Scientists and Engineers. Oxford University Press, New York.

Dyer, K.R., 1973. Estuaries: a Physical Introduction. John Wiley and Sons, New York.

Fulweiler, R.W., Nixon, S.W., Buckley, B.A., 2010. Spatial and temporal variability of benthic oxygen demand and nutrient regeneration in an anthropogenically impacted New England estuary. Estuaries Coasts 33, 1377–1390.

Giblin, A.E., Hopkinson, C.S., Tucker, J., 1997. Benthic metabolism and nutrient cycling in Boston Harbor, Massachusetts. Estuaries 20, 345–364.

Gross, T.F., Nowell, A.R.M., 1983. Mean flow and turbulence scaling in a tidal boundary layer. Cont. Shelf Res. 2, 109–126.

Gust, G., Muller, V., 1997. Interfacial hydrodynamics and entrainment functions of currently used erosion devices. In: Watts, J. (Ed.), Cohesive Sediments. Wiley, Chichester, pp. 149–174.

Hondzo, M., 1998. Dissolved oxygen transfer at the sediment-water interface in a turbulent flow. Water Resour. Res. 34, 3525–3533.

Jay, D.A., Uncles, R.J., Largier, J., Geyer, W.R., Vallino, J., Boynton, W.R., 1997. A review of recent developments in estuarine scalar flux estimation. Estuaries 20, 262–280.

Jorgensen, B., Revsbech, N., 1985. Diffusive boundary layers and the oxygen uptake of sediments and detritus. Limnol. Oceanogr. 30, 111–122.

Kalnejais, L.H., Martin, W., Signell, R., Bothner, M., 2007. Role of sediment re- suspension in the remobilization of particulate-phase metals from coastal sediments. Environ. Sci. Technol. 41, 2282–2288.
Kalnejais, L.H., Martin, W.R., Bothner, M.H., 2010. The release of dissolved nutrients and metals from coastal sediments due to resuspension. Mar. Chem. 121, 224–235.
Kim, S.C., Friedrichs, C.T., Maa, J.P.Y., Wright, L.D., 2000. Estimating bottom stress in tidal boundary layer from acoustic Doppler velocimeter data. J. Hydraul. Eng. 126, 399–406.
Kleeberg, A., Herzog, C., 2014. Sediment microstructure and resuspension behavior depend on each other. Biogeochemistry 119, 199–213.
Kornman, B.A., de Deckere, E.M.G.T., 1998. Temporal variation in sediment erodability and suspended sediment dynamics in the Dollard estuary. In: Black, K.S., Patterson, D.M., Cramp, A. (Eds.), Sedimentary Processes in the Intertidal Zone. Geological Society, pp. 231–241. Special Publications 193.
Koschinsky, A., Gaye-Haake, B., Arndt, C., Maue, G., Spitzy, A., Winkler, A., Halbach, P., 2001. Experiments on the influence of sediment disturbance on the biogeochemistry of the deep sea environment. Deep-Sea Res. II 48, 3629–3651.
Lippmann, T.C., 2013. Red Tide Disaster Relief Assistance: Bathymetric Surveying of Little Bay. Department of Environmental Services, New Hampshire, 2013. URL: http://des.nh.gov/organization/divisions/water/wmb/shellfish/red-tide/aquaculture.htm.
Lorke, A., Muller, B., Maerki, M., Wuest, A., 2003. Breathing sediments: the control of diffusive transport across the sediment-water interface by periodic boundary-layer turbulence. Limnol. Oceanogr. 48, 2077–2085.
Mitchener, H., Torfs, H., Whitehouse, R., 1996. Erosion of mud/sand mixtures. Coast. Eng. 28, 1–25.
Oczkowski, A., 2002. Riverine Inputs of Nutrients to the Great Bay, NH (USA). Master of Science thesis. University of New Hampshire.
Orlü, R., Frannson, J., Alfredsson, P., 2010. On near wall measurements of wall bounded flows – the necessity of an accurate determination of the wall position. Prog. Aerosp. Sci. 46, 353–387.
Percuoco, V.P., Kalnejais, L.H., Officer, L.V., 2015. Nutrient release from the sediments of the Great Bay Estuary, N.H. USA. Estuar. Coastal Shelf Sci. http://dx.doi.org/10.1016/j.ecss.2015.04.006 (in press).
Poppe, L.J., Paskevich, V.F., Williams, S.J., Hastings, M.E., Kelley, J.T., Belknap, D.F., Ward, L.G., FitzGerald, D.M., Larsen, P.F., 2003. Surficial Sediment Data from the Gulf of Maine, Georges Bank, and Vicinity; a GIS Compilation. USGS Open-File Report: 2003-1.
PREP, 2012. Environmental Data Report, Piscataqua Region Estuaries Partnership. University of New Hampshire. December 2012. URL: http://www.stateofourestuaries.org/.
PREP, 2013. State of Our Estuaries. Technical Report, Piscataqua Region Estuaries Partnership. University of New Hampshire, Durham, NH. URL: http://prep.unh.edu/resources/pdf/2013%20SOOE/SOOE_2013_FA2.pdf.
Sanford, L.P., Maa, J.P.-Y., 2001. A unified formulation for fine sediments. Mar. Geol. 179, 9–23.
Shepard, F., 1954. Nomenclature based on sand-silt-clay ratios. J. Sediment. Petrol. 24, 151–158.
Shields, A., 1936. Anwendung der ähnlichkeitsmechanik und turbulenzforschung auf die geschiebebewegung, vol. 26. Mitt. Preuss Versuchsanstalt fur Wassebaur und Schiffbau [Application of similarity mechanics and turbulence research to bedload movement.].
Short, F.T., Wyllie-Echeverria, S., 2009. Natural and human-induced disturbance of seagrasses. Environ. Conserv. 23, 17–27.
Sloth, N.P., Riemann, B., Nielsen, L.P., Blackburn, T.H., 1996. Resilience of pelagic and benthic microbial communities to sediment resuspension in a coastal ecosystem, Knebel Vig, Denmark. Estuar. Coast. Shelf Sci. 42, 405–415.
Soulsby, R.L., 1997. Dynamics of Marine Sands. Thomas Telford Services, Bath.
Statham, P.J., 2012. Nutrients in estuaries – an overview and the potential impacts of climate change. Sci. Total Environ. 434, 213–227.
Strickland, J., Parsons, T., 1968. A Manual for Seawater Analysis. Fisheries Research Board of Canada.
Sundbäck, K., Miles, A., Hulth, S., Pihl, L., Engström, P., Selander, E., Svenson, A., 2003. Importance of benthic nutrient regeneration during initiation of macroalgal blooms in shallow bays. Mar. Ecol. Prog. Ser. 246, 115–126.
Sundby, B., Anderson, L.G., Hall, P.O.J., Iverfeldt, A., Vanderloeff, M.M.R., Westerlund, S.F.G., 1986. The effect of oxygen on release and uptake of cobalt, manganese, iron and phosphate at the sediment-water interface. Geochimica Cosmochim. Acta 50, 1281–1288.
Swift, M., Brown, W., 1983. Distribution of bottom stress and tidal energy dissipation in a well-mixed estuary. Estuar. Coast. Shelf Sci. 17, 297–317.
Tengberg, A., Almroth, E., Hall, P., 2003. Resuspension and its effects on organic carbon recycling and nutrient exchange in coastal sediments: in situ measurements using new experimental technology. J. Exp. Mar. Biol. Ecol. 285, 119–142.
Tennekes, H., Lumley, J., 1972. A First Course in Turbulence. Massachusetts Institute of Technology, Boston.
Thompson, C.E.L., Couceiro, F., Fones, G.R., Helsby, R., Amos, C.L., Black, K., Parker, E.R., Greenwood, N., Statham, P.J., Kelly-Gerreyn, B.A., 2011. In situ flume measurements of resuspension in the North Sea. Estuar. Coast. Shelf Sci. 94, 77–88.
Thompson, C.E.L., Couceiro, F., Fones, G.R., Amos, C.L., 2013. Shipboard measurements of sediment stability using a small annular flume—Core Mini Flume (CMF). Limnol. Oceanogr. Methods 11, 604–615.
Tolhurst, T.J., Black, K.S., Paterson, D.M., 2009. Muddy sediment erosion: insights from field studies. J. Hydraul. Eng. 135, 73–87.
Tolhurst, T.J., Riethmuller, R., Paterson, D.M., 2000. In situ versus laboratory analysis of sediment stability from intertidal mudflats. Cont. Shelf Res. 20, 1317–1334.
Tolhurst, T.J., Black, K.S., Paterson, D.M., Mitchener, H.J., Termaat, G.R., Shayler, S.A., 2000b. A comparison and measurement standardisation of four *in situ* devices for determining the erosion shear stress of intertidal sediments. Cont. Shelf Res. 20, 1397–1418.
Tucker, J., Giblin, A.E., Hopkinson, C.S., Kelsey, S.W., Howes, B.L., 2014. Response of benthic metabolism and nutrient cycling to reductions in wastewater loading to Boston Harbor, USA. Estuar. Coast. Shelf Sci. 151, 54–68.
USGS, 2005. Marine and Coastal Geology Program Sediment Correlation Chart. Technical chart Open-File Report 2005-1001. United States Geological Survey. Woodshole, Massachusetts, United States. URL: http://woodshole.er.usgs.gov/openfile/of2005-1001/htmldocs/figures/c1f9chart.htm.
Warnken, K.W., Gill, G.A., Santschi, P.H., Griffen, L.L., 2000. Benthic exchange of nutrients in Galveston Bay, Texas. Estuaries 23, 647–661.
Wengrove, M.E., Foster, D.L., 2014. Field evidence of the viscous sublayer in a tidally forced developing boundary layer. Geophys. Res. Lett. 41, 5048–5090.
Widdows, J., Friend, P., Bale, A., Brinsley, M., Pope, N., Thompson, C., 2007. Intercomparison between five devices for determining erodability of intertidal sediments. Cont. Shelf Res. 27, 1174–1189.
Zhang, J.Z., Fischer, C.J., 2006. A simplified resorcinol method for direct spectrophotometric determination of nitrate in seawater. Mar. Chem. 99, 220–226.